LUNAR CRATER CENTRAL PEAK MINERAL MAPS - NEAR- AND THERMAL-INFRARED SPECTROSCOPY. E. Song[1], M. Lemelin[1], P. G. Lucey[1], B. T. Greenhagen[2], [1]Hawaii Institute of Geophysics & Planetology, University of Hawaii at Manoa (eugesong@higp.hawaii.edu), [2]Jet Propulsion Laboratory.

Introduction: Multispectral imagery of the lunar surface has become more abundant than ever in recent years, thanks to the suite of mission instruments with a variety of wavelength ranges and designs. In this study, we seek to refine the common spectroscopy-based techniques of mapping lunar mineralogy by incorporating multiple data sets together. The near- and thermal-infrared spectral ranges have different strengths and biases when it comes to identifying and measuring the abundances of the 3 most abundance lunar minerals - plagioclase, pyroxene, and olivine.

These minerals can be distinguished from each other from orbit by their diagnostic spectral features in the NIR, however the abundances of the two mafic minerals (pyroxene and olivine) relative to that of plagioclase are often skewed due to the weak spectral features of plagioclase being overwhelmed by the presence of olivine and/or pyroxene [1]. In the TIR, the Christiansen Feature (CF) provides some leverage to this situation, as it is equally sensitive to the 3 silicate minerals and is representative of the weighted sum of their modal abundances [Eq. 1].

We have developed a method of redistributing NIR mineral abundances using mineral maps derived from Kaguya Multiband Imager (method described in [2]) and CF maps from Diviner Lunar Radiometer on LRO. This method is applied specifically to crater central peaks, where peak material is thought to be uplifted crust or mantle and thus provide insight into the subsurface composition of the Moon. Central peak mineralogy has been studied extensively in both the NIR [2-4] and TIR [5], making them an ideal target for this study.

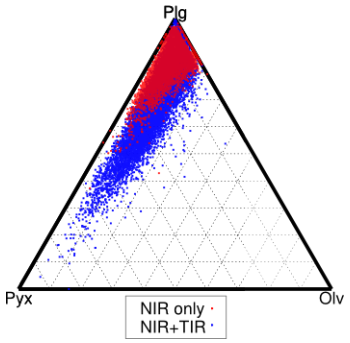

Figure 2, Ternary plot of Tsiolkovsky crater mineralogy before (red) and after (blue) the CF correction.

Data: The Kaguya Multiband Imager has 9 spectral bands ranging from 0.415 - 1.55 µm [6,7], and by using the newly-developed method discussed in [2] provides a pyroxene to olivine ratio for each pixel in the central peak (the individual abundance values for these mafic minerals are vulnerable to the plagioclase bias, but the ratio is not).

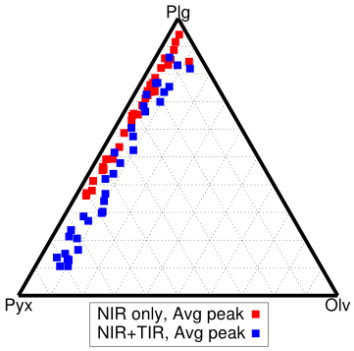

Figure 1, Ternary plot of the average plag, pyx, and olv abundances of each crater central peak before (red) and after (blue) the CF correction.

The CF value is derived from 3 bands on the Diviner instrument that are centered around 8 µm (CF values range from ~7-10 µm). The Diviner data is constrained to daytime-only, and both data sets are binned at 128 ppd. We applied the correction from [8] to the CF data, and kept each orbit strip separate until the last step of processing to minimize errors due to variations in the CF value's sensitivity to local time variations.

The craters included in this study are from Cahill et al., constrained to -50:50° latitude to optimize CF data quality.

Method:

Equation 1 shows the measured CF value (CF_{meas}) as the sum of the endmember CF values (known) weighted by their abundances (P, unknown), a value from 0-1.

$$CF_{meas} = CF_{pl}P_{pl} + CF_{pyx}P_{pyx} + CF_{ol}P_{ol} \quad \textit{Eq.1}$$

Where CF_{plg} = 7.98 µm (adjusted from 7.85 µm in lieu of a CF maturity correction, see *Future Work* section), CF_{pyx} = 8.125 µm, and CF_{olv} = 8.92 µm.

With the assumption that the NIR-based *ratio* of pyroxene to olivine (R) is well-constrained, we can solve for the abundances of each endmember [Equation 2-4] as a function of the measured CF value and the ratio R.

$$\frac{P_{pyx}}{P_{ol}} = R \;\rightarrow\; P_{ol} = \frac{P_{pyx}}{R} \quad \textit{Eq. 2}$$

$$P_{pl} + P_{pyx} + P_{ol} = 1 \;\rightarrow\; P_{pl} = 1 - P_{pyx}\left(1 + \frac{1}{R}\right) \quad \textit{Eq.3}$$

$$CF_{meas} = CF_{pl}\left(1 - P_{pyx}\left(1 + \frac{1}{R}\right)\right) + CF_{pyx}P_{pyx} + CF_{ol}\left(\frac{P_{pyx}}{R}\right)$$

Eq.4 $$\rightarrow \quad P_{pyx} = \frac{(CF_{meas} - CF_{pl})}{CF_{pyx} - CF_{pl} + \frac{CF_{ol} - CF_{pl}}{R}}$$

New values for $P_{pl,pyx,ol}$ were calculated for each CF orbit (anywhere from 6-26 orbits per crater, depending on the size of the peak and Diviner data coverage), then flattened simply by averaging the map layers. This method will improve with time by culling down the Diviner orbits to a smaller range of local times or applying some method of normalization to make them more uniform before flattening.

Preliminary Results:

Figure 1 shows the averaged peak mineralogies before and after the CF adjustment. The range of compositions, especially in the Plg-Pyx axis, has widened with the correction. This effect is demonstrated in the ternary plot of Tsiolkovsky crater [Fig. 2], and the mineral maps [Fig. 3] show where the changes were most drastic.

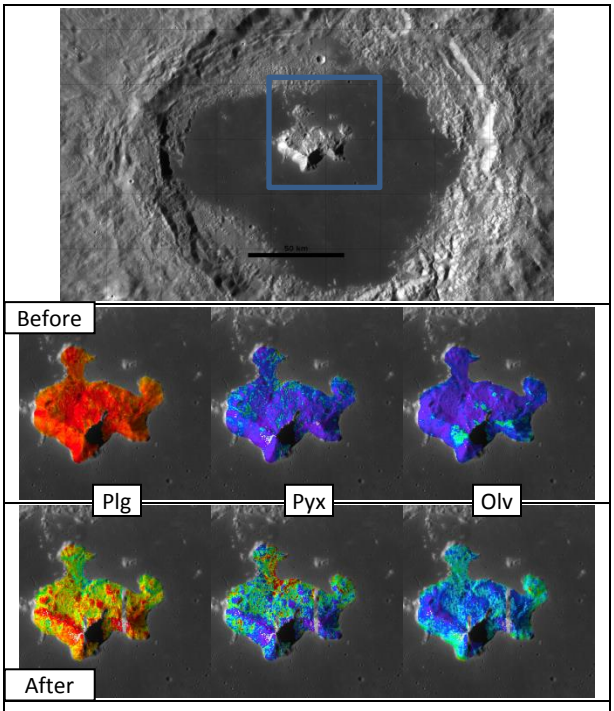

Figure 3, Tsiolkovsky crater. Background is LROC WAC. Top: original NIR abundance maps. Bottom: CF-adjusted abundance. Left: Plagioclase (0.0-0.9 stretch). Middle: Pyroxene (0.0-0.5 stretch). Right: Olivine (0.0-0.3 stretch)

The CF-adjusted maps also show better correlation with the new crustal thickness maps from GRAIL [9], shown in Figure 4 in terms of Proximity to the Mantle, a metric from [4] that is based on crustal thickness and the peak's depth of origin (a function of crater diameter). This could indicate that the lunar crust becomes more mafic with depth, which could not be validated with a similar study of central peaks using only CF values as a measure of crustal composition [5].

Future work. Still in development is a space weathering correction for the Diviner CF value, which has shown to increase the CF value with more mature surfaces. Because the CF endmembers listed above are based on laboratory measurements of relatively immature samples, they may be refined as well.

References:

[1]Issacson P. J. et al. (2011) *Meteorit. & Planet. Sci., 46,* 228-251. [2]Lemelin M. et al. (2014) *LPSC 2014, Submitted.* [3]Tompkins S. and Pieters C. M. (1999) *Meteorit. & Planet. Sci., 34,* 25-41. [4]Cahill J. T. S. et al. (2009) *JGR, 114,* E09001. [5]Song E. et al. (2013) *JGR, 118,* 689-707. [6]Ohtake M. et al. (2010) *Space Sci. Re., 154,* 55-77. [7]Kodama S. et al. (2010) *Space Sci. Re., 154,* 79-102. [8]Greenhagen B. T. et al. (2011) *LPSC 2011,* Abstract #2679. [9]Wieczorek M. A. et al. (2012) *Science, 8,* 671-675.

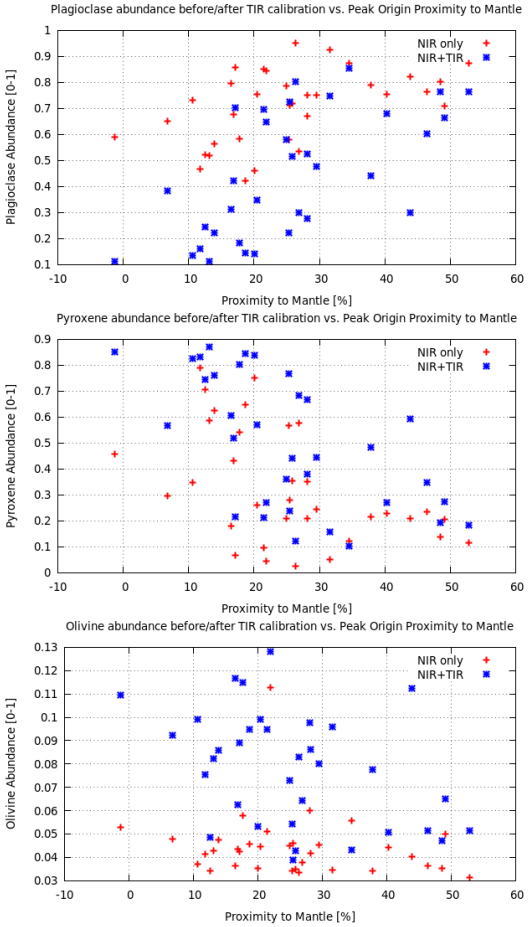

Figure 4, Averaged crater mineral abundances vs. central peak proximity to mantle. Red points are original NIR abundance; blue points are CF-adjusted.